SAG: Stars and Galaxies **Vol. 7**, id. 1, 2024 December 28

Long-term evolution of the Hα emission line of Pleione between Jan 2009 and Mar 2023 in the BeSS database II. Detailed profile variation during the periastron phenomenon

Junichi Katahira
Sakai-city, Osaka 591-8021, Japan
atak@db3.so-net.ne.jp

(Received 2024 September 28; accepted 2024 November 13)

Abstract

Using the Hα double peak emission lines of Pleione in the BeSS database from January 2009 to March 2023, the following points are discussed: 1) A comparison of the emission line profile variations observed at each periastron passage of the companion star reveals a striking similarity in the patterns of variation over the period 2015–2021. 2) As the periastron passage of the companion is repeated, the blue emission wing becomes stronger than the red emission wing towards the end of the Be-shell phase. 3) The mechanistic regularity whereby the red emission peak becomes earlier and stronger than the blue emission peak for a short time at each periastron passage of the companion star is interpreted qualitatively in terms of both the periastron position of the companion and the position of the disk in the celestial plane, as well as the tidal action of the companion star.

Key words: stars:Be star — stars:Pleione — stars:Be disk

1. Introduction

Pleione (28 Tau, BU Tau, HD23862) is one of the most luminous members of the Pleiades, with a magnitude of $V = 5.09$ and a spectral type of B8Vne (Ducati 2002). It has been identified as a Be-type star for over 130 years, exhibiting a normal B-type spectrum and recurrent episodes of disk formation activity with a 35-year cycle. During these active periods, the star undergoes a transformation in its spectral phase, shifting from the Be-shell phase to the Be phase approximately every 17 years (Cramer et al. 1995; Hirata 1995; Tanaka et al. 2007). Radial velocity analysis has demonstrated that the system is a single-line binary with an orbital period of $P = 218$ days and an eccentricity of e = 0.6–0.75 (Katahira et al. 1996; Nemravová et al. 2010).

As the temporal resolution of Pleione's observations was refined, significant variations in the Hα emission line profile were confirmed when the companion star reached periastron, thereby demonstrating the strong interaction between the disk and the companion star, and the existence of a large eccentricity (Pollmann & Vollmann, 2014). Subsequently, the synchronisation between the Hα emission line and the Hβ emission line was confirmed during the periastron (Katahira et al. 2020; Iliev et al. 2023). These observations were made under the condition that the state of the Hβ long-term variation V/R is less than one. However, further research across a wide wavelength range is required to extend these findings.

The Pleione Hα spectroscopic observation data from the early 2000s, including the data of Pollmann and Vollmann (2014), are accessible in the BeSS database[1]. Katahira (2023) selected 520 Pleione observations with wavelength resolution R = 10000–20000 for the period 2009–2023 from the database, and investigated the long-term evolution of the Hα emission line over 14 years in terms of parameters such as emission line peak intensities and radial velocities. It has been shown that it is possible to distinguish between periods of pronounced profile change (the periastron phenomenon), which occur at each periastron, and periods when this change diminishes (the long-term *background* variation). Henceforth, Katahira (2023) will be referenced as paper I.

This paper employs the spectra normalised in paper I to facilitate a more comprehensive understanding of the repeated periastron phenomenon. In section 3, we present a detailed analysis of the variations in the emission peak and wing regions during the periastron phenomenon, and investigate the similarity of the profile variation pattern for each periastron. In section 4, we present a qualitative discussion of the distinctive and mechanistic regularity whereby the red emission peak becomes earlier and stronger than the blue emission peak for a short time at each periastron passage of the companion star, as shown in section 3. This discussion is conducted in terms of both the position of the periastron and the position of the disk in the celestial plane, as well as the tidal action of the companion star.

[1] BeSS database ⟨http://basebe.obspm.fr/basebe/⟩

2. Observations used and their processing

In paper I, we employed a data set comprising 520 spectra from the BeSS database. The average *R*-value distribution of the selected observations is mostly around 15000. The data were subsequently normalised to the continuum level and converted to heliocentric wavelengths λ(helio; Å). In this paper, we have conducted further corrections to these spectra for orbital motion, utilising the binary orbital motion parameters proposed by Nemravová et al. (2010) through the application of the IRAF software. All calculations are based on data that have been converted from wavelength λ(helio) to wavelength λ(orbit). For purposes of clarity, the profile plots are presented in velocity scale.

In the correction work for the orbital motion, as the radial velocity Vr(G) of the centre of mass of the spectroscopic binary system remains undetermined, for the sake of simplicity, Vr(G) is set to zero kilometers per second. The radial velocity of Pleione (6.9 km s^{-1}: Pearce & Hill 1975, 5.1 km s^{-1}: Gontcharov 2006) is typically assumed to be approximately equal to the radial velocity of the Pleiades star cluster, Vr(Pleiades). The GAIA satellite has observed that Vr(Pleiades) is equal to 5.54 km s^{-1} (Gaia Collaboration 2018). It can be considered that there is no significant discrepancy between Vr(G) and Vr(Pleiades).

3. Analysis and Results

3.1. Details of Hα profile variations during Periastron phenomenon

Figure 1 illustrates the long-term variations in the blue and red peak intensities (*I_B, I_R*) of the Hα emission line and the minimum intensity (*I_c*) at the centre of the line from January 2009 to March 2023. The vertical green line indicates the periastron time of the companion star, which is based on the orbital motion solution 3 of Nemravová et al. (2010). This figure is referenced from paper I figure 1. Furthermore, this figure depicts the historical evolution of the periastron phenomenon. To provide an overview and to correlate the periastron phenomena, the observations are numbered at the time of periastron, with the number n = 1 denoting the time of the periastron in July 2005.

The group of profiles observed with Periastron number n = 25 is notable for its high concentration of the observation in figure 1, and has been observed with a high time resolution of almost one day. In paper I, the period during the periastron phenomenon was estimated from approximately -15 to +100 days based on the periastron time. The group of n = 25 observations also encompasses the entirety of the estimated period of the periastron phenomenon. It can therefore be concluded that the group of n = 25 observations represents the standard for investigating long-term changes in profile variations, as demonstrated repeatedly by Pleione.

Figure 2 illustrates the progression of profile variations across the entire dataset for n = 25. In order to facilitate the visualisation of profile variation patterns, the intensity scale has been adapted and the data have been classified into four groups. The horizontal axis represents the velocity scale, the vertical axis depicts the relative intensity, and the observation dates are listed on the right side of the figure in correspondence with the profile colours. Some italic numbers in parentheses in the date display indicate the phase of the orbital motion ϕ(orb). The figure captures the initial peak intensity variation during which the "$I\_B < I\_R$" state of the profile occurs, a transient increase in blue wing intensity indicated by the black arrow, and the appearance of the flat red emission peak indicated by the green arrow. The figure also provides an overview of the periastron phenomenon, which is characterised by a variation in the Hα double emission peaks region, oriented towards the central region of the line, for approximately one month from the periastron time.

Although the detailed variations are read out from figure 2, the characteristics of the variations are summarised below.

(1) Cataclysmic period (profiles in figure 2a)

The pre-periastron comparative profiles are included to illustrate the state of the emission profile ($I\_B > I\_R$). Following the periastron, the emission peak intensities reach their maximum values. Subsequently, a decline in intensity is observed one day after reaching the maximum. It is noteworthy that the onset of the periastron phenomenon initially exhibits a transitional phase spanning approximately 10 days, during which the "$I\_B < I\_R$" state of the profile is observed. It is also notable that the variations display the following additional characteristics: (i) the spacing between the emission line peaks tends to narrow; (ii) as the *I_c* increases above the continuum level, its velocity (*I_c*) initially shifts to the red, and then immediately begins to return to the blue; and (iii) there is a striking asymmetry in the profile of the central region of the line where *I_c* variations are observed. Moreover, a transient "wing-rising" phenomenon is observed in the blue emission wing region (velocity = -180 km s^{-1}), indicated by the black vertical arrow in figure 2. This occurs approximately 10 days after the periastron time. The position of this bulge in the blue emission wing shifts towards the red side over time and then disappears, showing a curious change. The phenomenon is linked to the rise in the red emission wing (approximately velocity = +180 km s^{-1}), though discernment is relatively straightforward, potentially due to the minimal variations in the blue emission wing.

(2) The period when a flat red emission peak appears in the line (profiles in figure 2b)

As the intensities of both emission line peaks decrease, a spike-like component emerges on the blue side of the red emission peak. On a daily basis, this component undergoes a process of weakening and eventual disappearance, with the red emission peak transitioning into a discernible flat shape. Once the flat shape peak has disappeared, the normal red emission peak becomes apparent. As the red emission peak continues to weaken, the "$I\_B > I\_R$" state that preceded the periastron phenomenon re-emerges. As *I_c* becomes weaker below the level of the continuum, the velocity (*I_c*) shifts to the blue side of the central minimum of the comparative profiles.

(3) Restoration period 1 (profiles in figure 2c)

The pronounced variations subside and the intensities of the two emission peaks gradually decrease. The intensity of *I_c* decreases to a level below that of the comparative profiles, while velocity (*I_c*) shifts back to the red side of the central minimum of the comparative profiles again.

(4) Restoration period 2 (profiles in figure 2d)

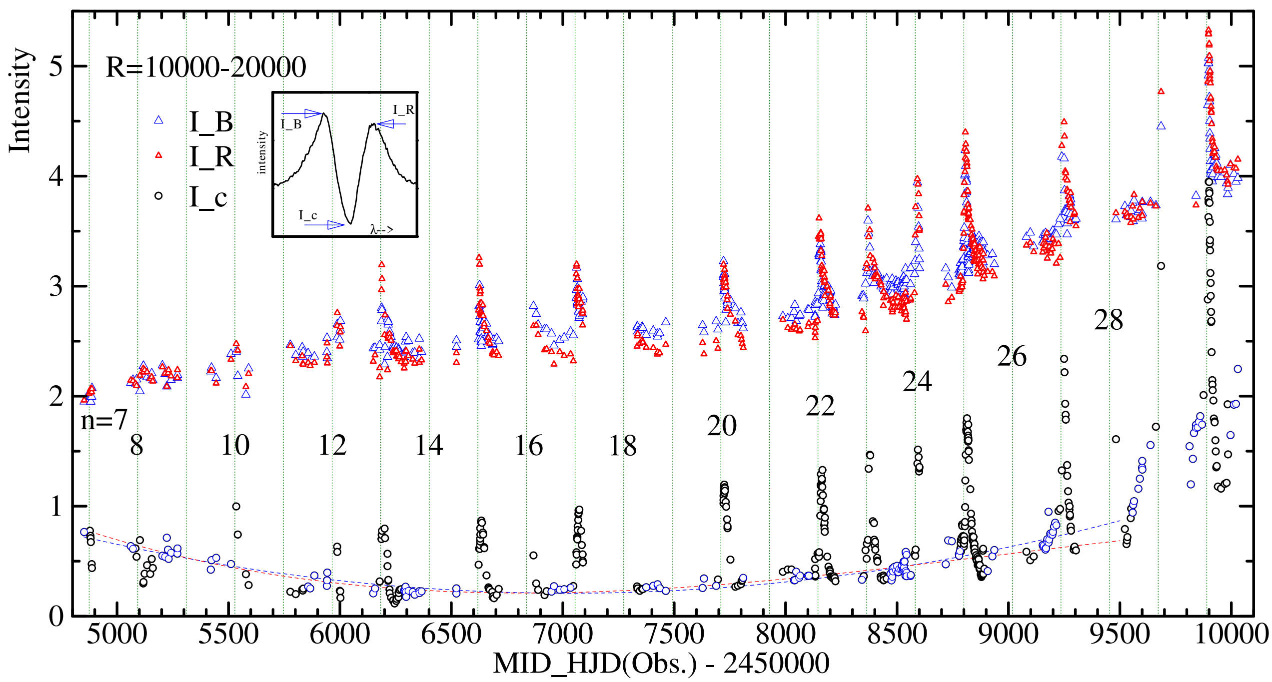

Fig. 1. Long-term intensity variation of the blue peak *I_B*, red peak *I_R*, and central minimum *I_c* of the Hα double peak emission line in 2009–2023. The horizontal scale subtracts 245000 from the heliocentric median time JD of observation. The vertical green line indicates the periastron time of the companion star, which is based on the orbital motion solution 3 of Nemravová et al. (2010). To facilitate overview and association, the observation groups are numbered at the time of periastron. This figure is referenced from paper I figure 1.

The intensities of the two emission peaks gradually decrease and approach those of the comparative profiles. The intensity of *I_c* increases and the velocity (*I_c*) returns to its original value, close to that of the comparative profiles.

3.2. *Range of Periastron n showing similar variability to n = 25 profile variability*

As previously reported by Honda and Katahira[2], analogous variations to the $n = 25$ variation pattern (figure 2) were observed in the $n = 22$ case. By extending such an analysis to other periods of the periastron phenomenon where $n = 25$ comparable cases occur, we can enhance our comprehension of the underlying mechanism of the companion tidal force. The following section will examine the appearance of three special features shown in figure 2 for each periastron phenomenon. These are: (1) the variation of the red peak becoming stronger than the blue peak immediately after periastron (hereafter abbreviated as "red peak preferential change"), (2) the "flat red emission peak", and (3) the "short-term rise in the blue wing", which is visible only for a few days, approximately 10 days after periastron. In view of the fact that the three profiles exhibit specific shape variations, the corroboration of their appearance at the n-th periastron provides substantiation for the existence of analogous profile variations, as depicted in figure 2.

3.2.1. *Occurrence of "red peak preferential change"*

As illustrated in figure 1, this is a distinct and fixed variability that is observed during the companion's periastron and is consistent across each periastron from $n = 13$ onwards. This estimation encompasses the periastron times when Pleione was not observable. It should be noted that no observations were conducted immediately following periastron at $n = 12$. Nevertheless, comparable variations in the intensity of the emission peaks are apparent, indicating that the same variability may occur at this periastron. Furthermore, it is noteworthy that this variation is not observed for $n \leq 10$.

3.2.2. *Occurrence of "flat red emission peak"*

The probable orbital phase of the appearance is estimated to be within ϕ(orb) = 0.070–0.095, and the profiles observed during this phase period for each periastron phenomenon are presented in figure 3. The colours of the drawn profiles follow the order of ϕ(orb), with blue being the early observation, black the middle and red the end. A single observation is black. Before $n = 12$, the total number of observations of periastron phenomenon is itself small. While the sample size of observations at $n = 30$ is substantial, the appearance of the "flat red emission peak" remains unclear. The $n = 17$ periastron phenomenon occurred during the period of maximum shell activity. Figure 3 indicates that the "flat red emission peak" was observed during periastrons $n = 17$–27. This estimation also encompasses the periastron times when Pleione was not observable, or not observed within the specified orbital phase interval. The "flat red emission peak" was observed during 11 periastron times, which represent approximately one-third of the number of periastron times repeated during the Be-shell phase.

[2] Honda, S., & Katahira, J. 2018, 日本天文学会 2018 年秋季年会講演 (No.N07a)

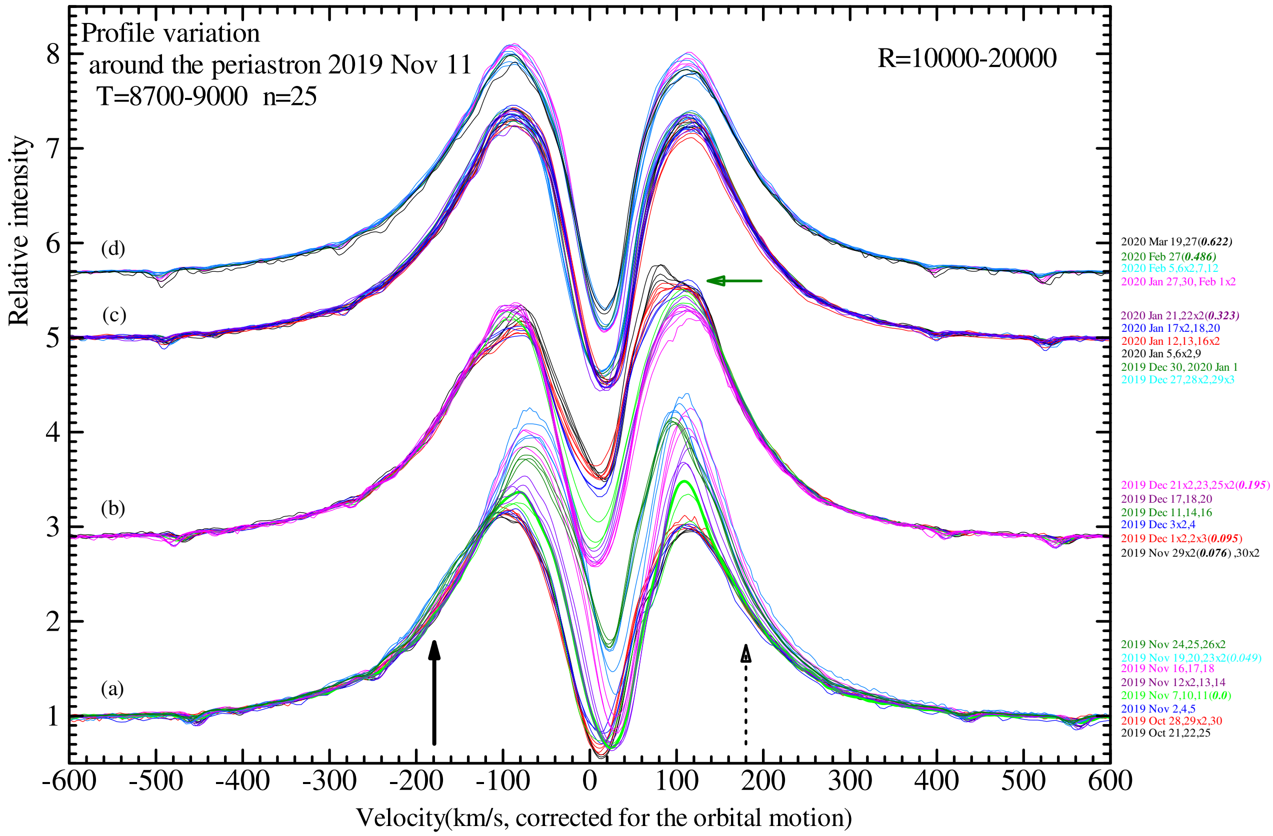

Fig. 2. Typical profile variation patterns in the periastron phenomenon. The group of observations with Periastron number n = 25, illustrated in figure 1, exhibits the highest time resolution and is representative of typical profile variations. For example, a distinctive profile morphology was documented during the course of the orbital motion phase, indicated by the green arrow, and the black arrow illustrates a detailed observation of a transient increase in the intensity of the blue wing. The observation dates are listed on the right side of the figure in accordance with the profile colours, and some italicised numbers in parentheses within the dates indicate the phase of the orbital motion ϕ(orb).

3.2.3. Occurrence of the "short-term rise in the blue wing"

The variation under consideration is indicated in figure 2 by the vertical arrow. This variation demonstrates that the wing intensity (at velocity = -180 km s^{-1}) appears to increase only for a few days. Due to the very limited observation period, this variation can only be visually confirmed for n = 22 and 30, which have a substantial number of observations. Accordingly, the following confirmation method, which employs the time course of the intensity, was utilised.

The confirmation method is based on the impression of intensity variations, indicated by the two vertical arrows in figure 2, which are easy to check visually. It was resolved that the discrepancy in the time of appearance of the intensity peak between the time series of the average intensity at velocity = -180 $\pm$ 11 km s^{-1} and the time series of the average intensity at velocity = +180 $\pm$ 11 km s^{-1}, as illustrated in figure 4, was utilised. In the same figure, the date markers have been added to correspond with the date information when the intensity is observed to increase. Figure 4 shows that the "short-term rise in the blue wing" can be interpreted as a delayed fluctuation in comparison to the rise in the red wing intensity. This presents a clear shift in the peak intensity period, although the mean intensity change is noisy. As illustrated in figure 5, the short-term rise in the blue wing is observed at n = 15, 22 and 30, in accordance with the aforementioned confirmation method. It seems probable that a shift in peak time was also observed at n = 13; however, this could not be adopted due to the considerable data variability. Note that a tendency for the intensity level of the red wing to be stronger than that of the blue wing in figures 4 and 5 is due to the choice of velocity position used for comparison.

3.3. Interpretation of the range of Periastron n, showing similar variations to those observed with n = 25

The observed appearance patterns for the n are as follows: (1) the "red peak preferential change" is observed in n = 13 – 30, (2) the "flat red emission peak" in n = 17–27, and (3) the "short-term rise in the blue wing" in n = 15, 22, and 30. The discrete n results in (3), constrained by the limited time observed, can be interpreted as n = 15–30. *Therefore, in the n = 17–27 cases, a similar profile variation to n = 25 is deemed to have occurred.* It can now be suggested that an attempt to interpret the profile change shown in figure 2 within the specified range of n = 17–27 in the same scheme is justified.

From an alternative perspective, the aforementioned similarity check for the periastron n would yield approximately four categories of disk-reaction pattern by the companion star at the

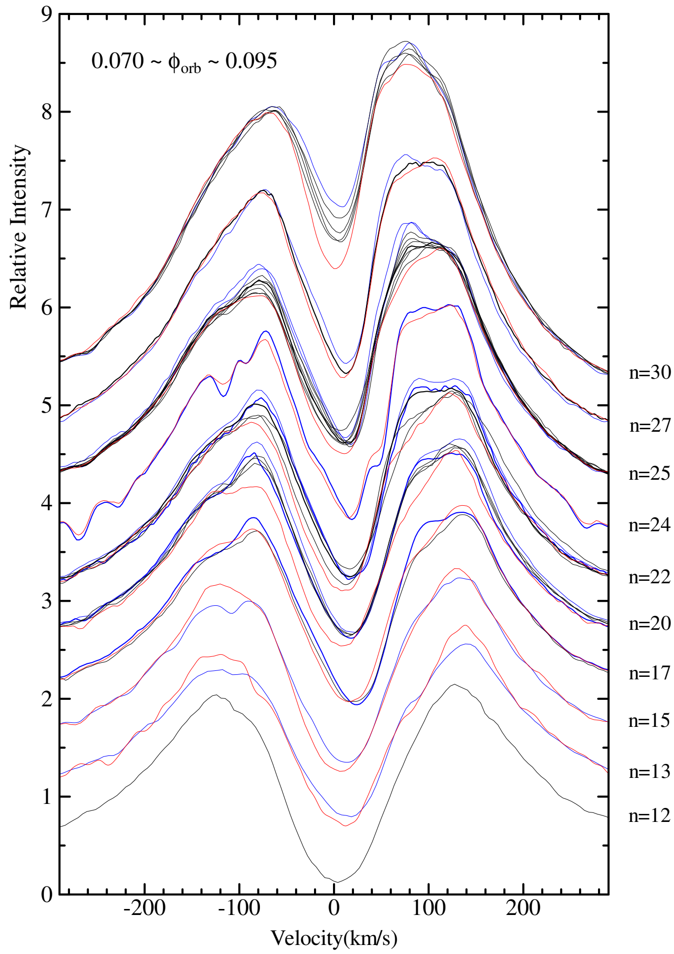

Fig. 3. Occurrence of "flat red emission peak". The central part of the emission line profile observed during each periastron phenomenon, between orbital motion phases ϕ(orb) = 0.070–0.095, is shown. The vertical axis shift for each group is adjusted accordingly. The colours of the drawn profiles follow the order of ϕ(orb), with blue being the early observation, black the middle and red the end. A single observation is black. The number n to the right side of the profile represents the periastron number. The "flat red emission peak" is observed for periastron n = 17–27.

periastron. These categories are as follows: **(i)** $n \leq 12$ cases, **(ii)** n = 13–16 cases, **(iii)** n = 17–27 cases, and **(iv)** n = 30 case. In the cases of periastron, n = 28 and 29, Pleione was not observable. The following analysis will proceed in an arbitrary order in order to facilitate an examination of the meaning of the four categories. It may be reasonably assumed that the most numerous *Category* (iii) is the case where, as the disk grows and undergoes precession, a similar emission line-forming environment is maintained as in n = 25. *Category* (iv) indicates the commencement of a modification of the environment conducive to emission line formation in *Category* (iii), as the transition to the Be phase is initiated. As documented in paper I, the ratio of the emission line peak intensities V/R of the long-term *background* variation approaches a value of less than 1, suggesting the change in the density distribution due to the progression of the density wave in the disk. It would appear that *Category* (i) represents a case where the disk growth is insufficient in comparison to *Category* (iii), and the tidal effect exerted by the companion star does not readily extend to the region where emission peaks are formed. Nevertheless, the pronounced decline in I_c at n = 8 unmistakably demonstrates the tidal influence of the companion star, as shown in figure 1. In accordance with the findings of Hirata (2007), the time of *Category* (i) is the period during which the south polar side of the disk is observed. Does a density distribution that more readily covers the south polar photosphere occur for a brief period during the periastron? Alternatively, could the change in disk inclination due to precession alter the tidal impact of the companion star? *Category* (ii) shows the "red peak preferential change" but no "flat red emission peak". For these two indicators *Category* (ii) is borderline to *Category* (iii). The transition from *Category* (i) to *Categories* (ii) and (iii) may provide insight into the tidal action of the companion star.

Figures 4 and 5 present a novel perspective on the periastron phenomenon, wherein the variability in the emission wing is also correlated with the emission peak variation. Additionally, figure 5 illustrates that long-term alterations in the blue and red wing intensities manifest when the periastron phenomenon subsides. In order to gain new insights into the variability of the entire disk, the long-term variations in the intensity of the emission wing are examined next.

3.4. *Long-term variations in the Hα emission wing*

In order to obtain the disk information from the emission wing, the same method of calculating the average intensity between $\delta\lambda$ = 0.5 Å, as employed in the creation of figures 4 and 5, is utilised. The four wing velocity positions on the blue and red sides of the emission wing are set as follows. The initial velocity positions are set as *group* (a), corresponding to the red and blue wing velocity data shown in figures 4 and 5. Secondly, the positions are considered as *group* (b), with velocities of $\pm$250 $\pm$ 11 km s^{-1} (6568.29 $\pm$ 0.25 Å, 6557.35 $\pm$ 0.25 Å). Thirdly, the positions are considered as *group* (c) with velocities of $\pm$340 $\pm$ 11 km s^{-1} (6570.25 $\pm$ 0.25 Å, 6555.38 $\pm$ 0.25 Å), situated in closer proximity to the continuum level. Furthermore, the velocities of +500 $\pm$ 11 km s^{-1} (6573.75 $\pm$ 0.25 Å) and -530 $\pm$ 11 km s^{-1} (6551.23 $\pm$ 0.25 Å) are situated at the continuum level, representing a fourth *group* (d). *Group* (a) shows the average

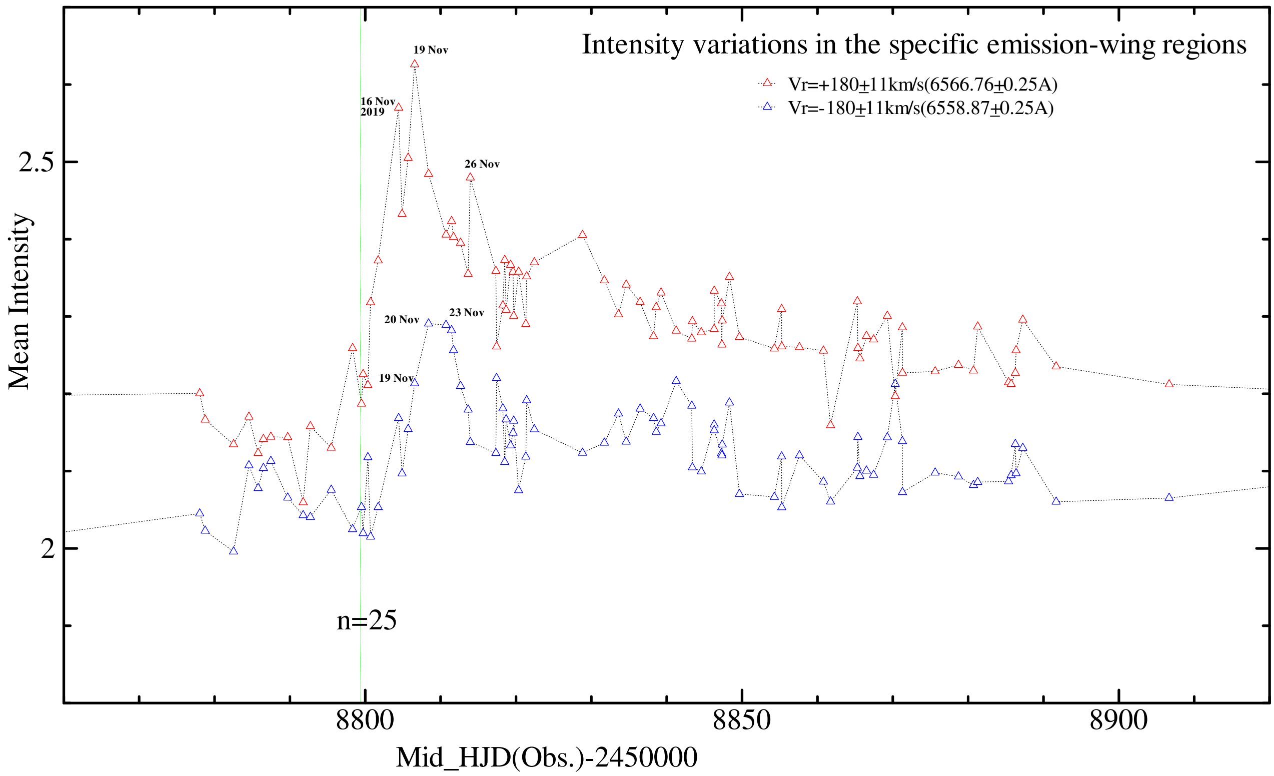

Fig. 4. Occurrence of "short-term rise in the blue wing" at $n = 25$. The vertical axis is the mean intensity change at the arrow positions in figure 2, where the added dates correspond to the profile observation dates in figure 2. The horizontal axis is the same modified JD as in figure 1. The blue △ marks with the dates "19 Nov–23 Nov" correspond to the period when the blue wing at the arrow in figure 2 is rising. Despite the considerable observational error, the time difference between the peak epochs indicated by the red and blue △-marked variations is likely to be discernible.

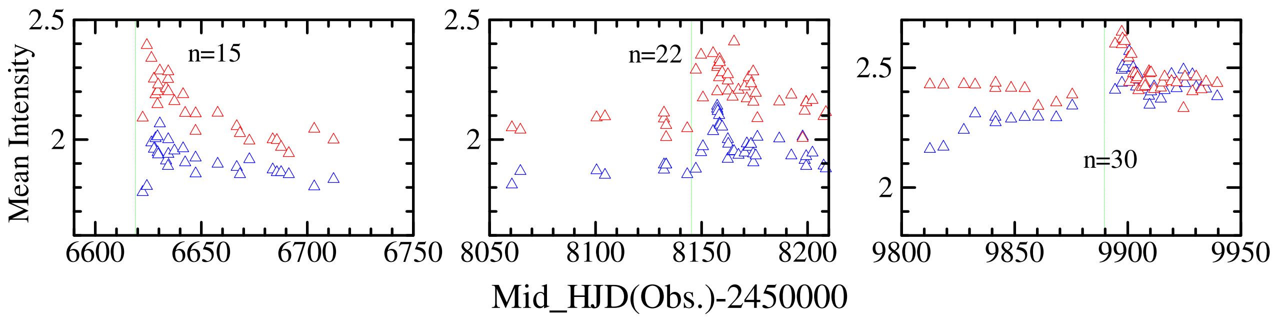

Fig. 5. Occurrence of the "short-term rise in the blue wing" at $n = 15$, 22, and 30. The red and blue △ marks are the same as in figure 4 and the green vertical line indicates the periastron time of number n. The three figures are examples where the time of appearance of the red and blue peaks and the discrepancy between the two peaks could be confirmed. Note that $n = 22$ and 30 are cases where the "short-term rise in the blue wing" could be confirmed visually.

intensity variation at the strong steep emission wings corresponding to black vertical arrows in figure 2, *group* (d) shows the average variation at the continuum level, *group* (c) shows the average intensity of the far wings just above the continuum level, and *group* (b) shows the average variation of the intermediate wing intensity at the midpoint between *groups* (a) and (c). In addition, *group* (b) is set to be in the regions where the steep emission wings occur from the background far wing intensity level. Each group, in the order of *groups* (a), (b), and (c), may correspond approximately to its different region of formation towards the inner region of the disk.

The results of the calculation are illustrated in figure 6, with the red and blue marks indicating the variation in the average intensity of the aforementioned red and blue side wings, respectively. It seems reasonable to conclude that the long-term variation in *group* (d) is indicative of the adequacy of the continuum position. The estimated error, $\delta I = \pm\, 0.02$, in *group* (d) was derived from the observed scatter of the data, and the error in *group* (c) was estimated to be of a similar magnitude. The errors in *groups* (a) and (b) were estimated based on the distribution of calculated values during the period when the periastron phenomenon subsided. The rationale for setting the displayed data in *group* (a) to $T > 5000$ is to ensure that the wing intensities at the velocities of ±180 km s^{-1} exhibit sufficient distinguishability from the variation of the emission peak intensities. It is difficult to guarantee that the Earth's atmospheric water vapour absorption does not overlap when determining the wing velocity position. *Group* (b) is significantly influenced by water vapour absorption.

The following two aspects of the intensity variations observed in the emission wing depicted in figure 6 will be examined.

[1] *Groups* (a) and (b) exhibit a discernible correlation with the variation in emission peak intensity (figure 1) immediately following periastron passage, whereas *group* (c) displays a less pronounced correlation. This trend indicates that the tidal effects of the companion star may extend to the inner region of the disk, given that the tidal action of the companion star causes the periastron phenomenon. In paper I, the correlated linkage between the variability of the Hβ emission line peak intensity (velocity (Ipeak) $\cong \pm130$ km s^{-1}) and that of the Hα emission line peak was interpreted in a similar manner.

Nevertheless, given that it is an interlocking pattern (positively correlated) within the Hα emission line, an alternative viewpoint is also possible. It has been proposed that the spreading of the Hα emission line wings in Be-type emission line stars is due to electron scattering in the disk (Poeckert & Marlborough 1979; Marr et al. 2022). Following this, it seems simple to infer that the linkage observed in figure 6 is due to the temporary intensification of the Hα emission line peak, which is transmitted to the wing region of the same line by electron scattering effects within the disk. If this is indeed the case, the phenomenon of a "short-term rise in the blue wing" (discussed in sub-subsection 3.2.3) must be regarded as an "echo effect" of the enhancement in emission peak intensity on the wing region just after the periastron. Interestingly, the same section, sub-subsection 3.2.3, proposes that the phenomenon of a "short-term rise in the blue wing" may have originated at periastron number n = 13. This would be related to the observation that I_R and I_B began to exhibit more pronounced variations at n = 13 than previously, as illustrated in figure 1. Such a correspondence may indicate the emergence of an "echo effect". However, as described in subsection 3.1, the rationale behind the shift in the "wing-rising" position towards the red side over time remains unclear. The "echo effect" does not provide an explanation for the observed redward shift.

[2] In the long-term *background* variations exhibited by the *groups* (a), (b), and (c), there is a discernible strengthening of the blue and red wing intensities from approximately T = 7800. Furthermore, a reversal in the intensity of the blue and red wings is observed in the *groups* (b) and (c). This variation is indicative of the observation that the profile intensities begin to exhibit asymmetry in the blue and red wings as they intensify (see also figure 2). Note that at approximately T = 7800, the ratio of emission peak intensities V/R reaches its maximum in the long-term *background* variation. The correlation between V/R variability and wing asymmetry in Pleione is unclear, but this trend is a new finding in the current "Be-shell" phase, and will be discussed later.

The increase and asymmetry in the emission wing intensity, as mentioned in [2] above, is not easy to read in figure 6. For a more simple representation, the total width and bisector at emission wing intensity I = 1.5 are illustrated in figure 7. The calculation process for figure 7 is based on a cubic approximation of the wing in the range of emission line intensity I = 1.2–1.8, using the least-squares method. Although the intensity of the emission line at the I = 1.5 level is markedly influenced by the H_2O blend, it is evident that at $T > 7800$ the bisector position in the long-term *background* variation demonstrates a discernible shift towards the blue side, accompanied by an increase in the total width of the emission wing. To illustrate this situation corresponding the profile variation, the emission line profiles in the vicinity of T = 9900 are presented in figure 8. Additionally, the emission line profiles depicted in Marr et al. (2022), figure 1 (19/12/2018 & 18/12/2019), which roughly correspond to T = 8500 and 8800 in figure 7, respectively, also exhibit a similar trend to that observed in figure 8.

In paper I, during the long-term *background* variation, the V/R variation of the double-peaked emission line was confirmed, albeit in a traceable way. In the calculation of the retrograde one-armed density wave, Okazaki (1996) showed that for an inclination of 60°, the red wing extends when $V > R$ and the blue wing extends when $V < R$. Although this behaviour was not shown in the figure for a inclination of 90°, a similar tendency can be postulated for a inclination of 90°. On the other hand, in the calculation of the prograde one-armed density wave, Hummel and Hanuschik (1997) figure 3 shows that the wing extends on the side of the stronger Hα emission line peak for the inclination i = 60°–90° disk. The wing extension patterns differ between the two calculations; however, symmetrical wing strengths are exhibited in the $V = R$ case. At approximately T = 7800 in figure 7, the value of V/R reaches its maximum and subsequently approaches V/R = 1 (at approximately T = 9800), which are shown in paper I figure 3. However, the blue emission wing extends, and no symmetry of the emission wing is observed, as illustrated in figure 8. From a phenomenological standpoint, it is reasonable to posit that discrete movements occur in both the emission line peak region

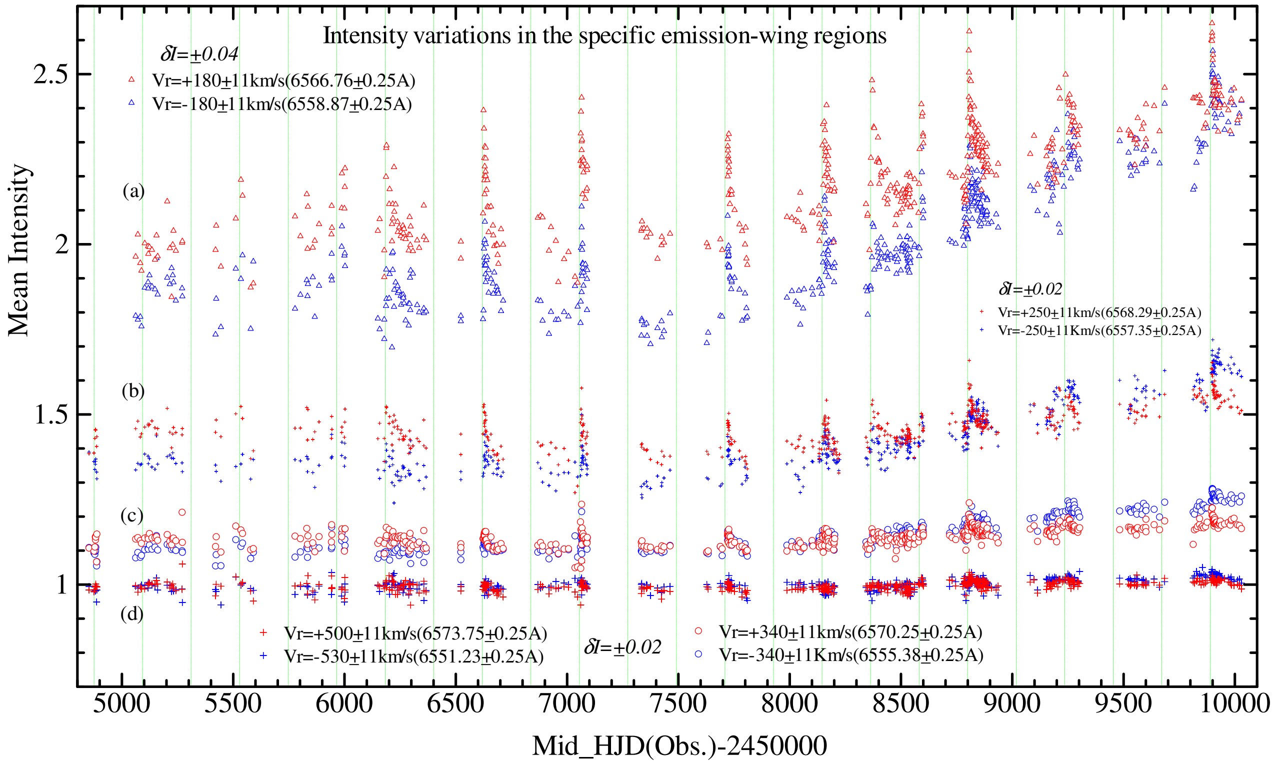

Fig. 6. Long-term variations in the average intensities of the red and blue emission wings. The average intensity is defined as the mean value over the ±0.25 Å range of wavelengths indicated in brackets on the velocity scale. The horizontal axis is the same modified JD as in figure 1. The vertical green line indicates the periastron time of the companion star. *Group* (a) illustrates the average intensity variation corresponding to the black vertical arrow in figure 2, *group* (d) depicts the variation at the continuum level, *group* (c) demonstrates the average intensity just above the continuum level, and *group* (b) presents the variation in the wing average intensity at the midpoint between *groups* (a) and (c). The measurement error, denoted by δI, is estimated from the variation in measurements observed during the period in which the periastron phenomenon subsided. The impact of H_2O absorption is considerable in *group* (b). It is notable that the V/R value of the emission peak intensities reaches its maximum around T = 7800 in the long-term *background* variation.

and the emission line wing region, respectively, potentially in the outer and inner regions of the disk.

In the previous Be epoch (1988–2004), Rivinius et al. (2006) figure B.4 shows how the extension of the emission wing changes from the blue to the red side wing from the profile variation between 1991 and 2003. Note that this is a change under an emission line peak intensity ratio $V/R < 1$, which can be also explained by Hummel and Hanuschik (1997). However, if the same phenomenon is observed in the forthcoming Be phase, it will be associated with the bisector in figure 7, which is inverted. If this is indeed the case, it would imply the existence of a spiral density wave.

4. Discussion

Figure 2 depicts the observations with the highest temporal resolution, including almost daily observations, among the data utilized from 2009 to 2023. It is clear that the red emission peak displays significantly greater variations than the blue emission peak from the time of periastron. This distinctive pattern persists for approximately 30 days. As illustrated in section 3, these emission peak variations are evident at n = 17–27 (from the shell maximum period to the end of the Be-shell phase) in figure 1. In particular, for all periastrons after n = 13, there is *an initial variation* in which the red peak first attains

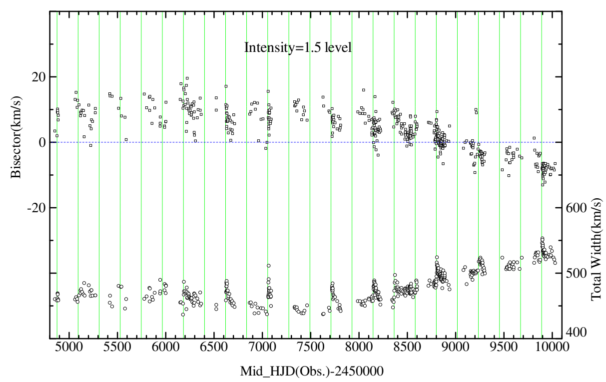

Fig. 7. Long-term variation of the bisector and the total width at the intensity of the emission wing I = 1.5. The left vertical axis depicts the bisector, while the right vertical axis represents the total width. The horizontal axis is the same modified JD as in figure 1. The vertical green line indicates the periastron time of the companion star. When examining the long-term *background* variation, a discernible shift occurs at $T > 7800$, whereby the total width of the wing develops and the bisector shifts towards the blue side. This indicates that the blue wing is beginning to extend.

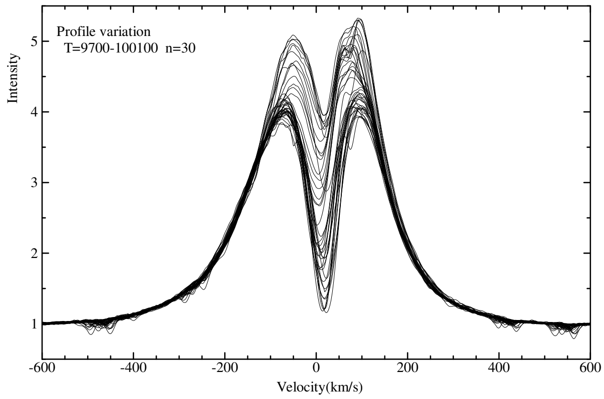

Fig. 8. Profile variation in the vicinity of $T = 9900$ ($n = 30$ in figure 1). Focusing on the wing, it is clear that the blue wing is more overhanging than the red wing. This is the period of $V/R = 1$ in the long-term *background* variation.

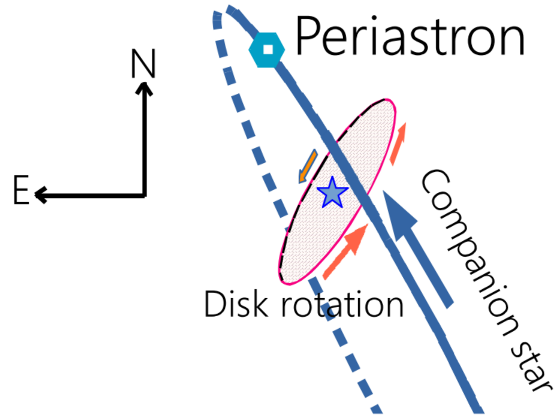

Fig. 9. Image of the positions of the Be-disk and the companion's periastron projected on the sky centred on the primary star (an imaginary sketch). The solid marks correspond to the front halves of the projected sky, and the dashed marks correspond to the rear halves. It is assumed that the position of the companion's orbital plane on the sky is in a NE–SW direction (see text for details).

a greater intensity than the blue peak at each periastron (i.e., the "red peak preferential change"). It is curious that this particular feature continues to manifest itself with such regularity. In addition, the ELODIE database[3] includes the periastron 14/12/2001 variations that occur at a time past the emission intensity maximum of the previous Be phase. These observations really confirm the "red peak preferential change". It is likely that , despite the phase transition from the current Be-shell phase to the forthcoming Be phase, this phenomenon will remain unaltered.

It would be intriguing to ascertain whether this "red peak preferential change" could be linked to an initial variation in the density distribution in the disk resulting from the tidal force during the periastron of the companion star. In order to facilitate more effective interpretation in the future, we have connected the related papers in subsections 4.1–4.3 below.

4.1. *Estimation for the positions of the Be-disk and the companion's periastron on the celestial plane centred on the primary star*

In light of the discussion presented in paper I, which follows the precession of the disk as outlined by Hirata (2007), it is possible to estimate that the inclination of the disk exhibiting the profile variation of figure 2 is approximately 72°. In this scenario, the configuration of the disk on the celestial plane centred on the primary star (referred to as sky) can be approximated as an intermediate arrangement ($\equiv$ *Disk Arrangement A*) between the disk arrangements "1980.90" and "1989.02", as illustrated in Hirata (2007) figure 2b.

Furthermore, Hirata (2007) figure 2a depicts the configuration of the companion orbital plane with respect to the sky. In the illustration, the great circle that is orthogonal to the disk precession axis (the axis connecting the plus sign and the centre of the celestial sphere) is indicative of the companion star's orbital plane. From the figure, it can be observed that the inclination i of the companion's orbital plane is nearly 90°, oriented approximately in a NE–SW direction on the sky. The direction in which the companion star moves on the sky has yet to be determined. However, assuming that the direction is the same as the direction of rotation of the star/disk, the companion star would appear to move from the SW to the NE. Moreover, radial velocity analysis of the binary system indicates an eccentricity of $e = 0.6$–0.75, and a longitude $\omega = 149°$–$157°$ of the periastron position (Katahira et al. 1996; Nemravová et al. 2010). From these values for the i, e, and ω it can be inferred that the position of the companion's periastron on the orbit can be interpreted as being in slight proximity to the observer in relation to the reference plane (celestial plane) of the centre of gravity of the binary system ($\equiv$ *Periastron Position on the orbit A*).

Using these concepts of the "*Disk Arrangement A*" and "*Periastron Position on Orbit A*" together, figure 9 shows how the visibility of both the Be-disk and the periastron position are plotted on the sky centred on the primary star, drawn by hand. The solid marks correspond to the front halves of the projected sky, and the dashed marks correspond to the rear halves. From the figure, it can be inferred that the companion's periastron is north of the primary star on the sky, and that the companion passes through the northern part of the disk at periastron and then orbits to the rear, the opposite side of the disk in a NE direction.

4.2. *Optically thin approximation of the outer region of the disk and Constant radial velocity contours on the disk*

The Hα emission line profile, formed by a Kepler-rotating optical thin Be disk, can be approximated by contributions from the neighbourhood of each constant radial velocity curve on the disk's equatorial plane. This approximation allows for a simple connection between the radial velocity contours and the emission line profile. As illustrated in figure 2, the profile variation observed during the periastron is representative of a disk with a considerable optical thickness[4] and an outer disk radius

[3] ELODIE database ⟨http://atlas.obs-hp.fr/elodie/⟩

[4] It is evident that in the case of optically thick Be disks, the treatment of radiation transfers within the disk must be conducted with the utmost rigour.

of $Rd \approx 20R_*$, as discussed in paper I. Nevertheless, when the short-term variations in the emission line intensity are qualitatively assessed during periastron, where the outer disk region makes a significant contribution, the optical thin approximation may be considered a reasonable zero-order approximation.

Figure 10 illustrates the constant radial velocity contours of the equatorial plane of the Kepler rotation disk, with an outer radius of $Rd = 20R_*$. The direction of the observer is aligned with the x-axis, corresponding to the right side. It is assumed that at the radius $r = 1R_*$, the disk is in contact with the photosphere and has a rotational velocity, V_0, of 420 km s^{-1}. This value was derived from the parameter Vc value for Pleione, as presented in Frémat et al. (2005) table 9. In the same figure, the contours of the constant radial velocity of ±70, ±100 km s^{-1}, and so forth are drawn in accordance with the velocity scales that delineate the peak intensity region in figure 2. It is assumed that the outer region of the disk represented by these contours is optically thin and that the observed short-term variation in peak intensity is related to the iso-radial velocity region. The *aim* is to consider the short-term variation of the peak emission intensity in a straightforward manner by superimposing the "disk figure" with the contours of constant radial velocity, as shown in figure 10, at the position of the "disk-mark" in figure 9.

Note that in paper I we pointed out the possibility of the one-armed density wave being activated in the disk, under which the shape of the constant radial velocity contours deviates considerably from the simple Kepler rotation case of figure 10 (Okazaki 1996; Hummel & Hanuschik 1997). However, since the present discussion is a qualitative , it is considered simplistic.

4.3. *Speculation on the mechanism of the "red peak preferential change" for each periastron*

Figure 9 suggests that the companion passes through the northern part of the disk at periastron and then orbits to the rear, the opposite side of the disk in a NE direction, as considered in subsection 4.1. The contour of the constant radial velocity of +100 km s^{-1}, corresponding to the intensity of the red emission peak, as illustrated in figure 2, extends into the outer region of the disk north of the star, as demonstrated in figure 10. It can be proposed that the region of the disk in the northern outer region, where the red emission peak forms, would be affected at each periastron.

Then, we naturally suppose that the warping may occur in the northern and southern outer regions of the disk on either side of the primary star as a consequence of the tidal force exerted by the companion. This could extend the area of the outer disk visible to the observer in the warp phenomenon, which would result in an increase in the emission line peak intensity. Nevertheless, it is difficult to envisage a consistent mechanism that would generate the "red peak preferential change" and the subsequent profile variations in only the warp phenomenon.

In the case of Pleione Be disks, Hirata and Kogure (1978) estimated the optical thickness of the Hα line to be approximately 2000 in November 1976. This analysis was conducted four years after the onset of the active phase of disk formation, when the disk had reached an outer radius of 8.4 R_* (Hirata & Kogure 1978; the conversion value of Re(Hα) with j = 1/2). Even at this occasion, the optical thin approximation is not appropriate.

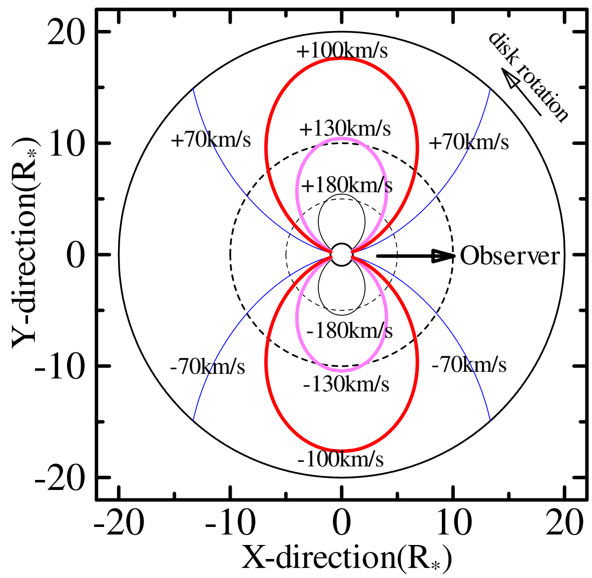

Fig. 10. Constant radial velocity contours of the equatorial plane of the Kepler rotating disk. A rotational velocity V_0 = 420 km s^{-1} at the radius $r = 1R_*$ is adopted. Under the assumption of an optical thin disk, the constant radial velocity contours extending into the outer region of the disk are assumed to correlate with the blue and red emission line peaks on the velocity scale.

Conversely, if a formation and subsequent disappearance of the special density distribution in the outer region of the disk is observed at each periastron, the profile variation may be more readily explained. In the following, we will consider this latter possibility.

The effect of the periastron passage of a companion star on the density structure of a circumstellar disk is studied by Panoglou et al. (2016a, b) under conditions of co-planar alignment and prograde motion in a binary system, using a smoothed particle hydrodynamics (SPH) simulation approach. The calculation with an eccentricity of e = 0.6, corresponding to that of Pleione, indicates the formation of a *two-spiral-arms* density structure upon the arrival of the companion at the periastron. This formation occurs in both the disk portion neighbouring the companion star and the disk portion opposite the primary star. This phenomenon significantly alters the density distribution throughout the disk. Additionally, the structure rotates in conjunction with the motion of the companion and ceases to exist upon the departure of the companion from the disk (cf. Okazaki et al. 2002). Furthermore, the calculation with an eccentricity of e = 0.0 indicates the presence of a similar density structure exhibiting a locked motion to the rotation of the companion in the outer regions of the disk.

In view of the aforementioned papers, we would like to examine the mechanism of the "red peak preferential change" at each periastron, as shown by Pleione. Unfortunately, the tilt of the companion's orbital plane to the Pleione disk does not match the model in the simulation of Panoglou et al. (2016a, b). The Pleione disk is nearly orthogonal to the companion orbital plane due to precession (Hirata 2007). Nevertheless, due to the appeal of studying the density changes of the disk associated with the periastron position of the companion, we will attempt to make the following speculative and tentative inferences ((1) and (2)) on the basis of the findings in Panoglou et al. (2016a, b).

(1) It is assumed that even if the tilt of the companion's orbital plane to the disk is approximately 90°, the tidal action of the companion will excite a *two-spiral-arms* density structure in the outer region of the Pleione's disk after periastron passage. Furthermore, it is assumed that this structure does not significantly alter the density distribution of the entire disk. This second assumption is analogous to the calculation of eccentricity $e = 0.0$ case presented by Panoglou et al. (2016a, b). In accordance with the above assumptions, it is postulated that a *two-spiral-arms* density structure will emerge in the outer region of the disk, as illustrated in figure 9, in NE of the primary star and in the opposite direction. The reason of this selection is that in this outer region, NE of the primary star, the rotational directions of the disk and the companion are not aligned, but are not colliding. The configuration may be regarded as being relatively close to the state of co-planar alignment of the binary system adopted in Panoglou et al. (2016a, b). These regions of the structure correspond to the outer region of the disk exhibiting radial velocities of ± 100 km s^{-1} in figure 10, which are the formation regions of the red and blue peak intensities, respectively. These assumptions will yield the following result: the region of emission line formation at the outer region of the disk will increase due to the emergence of the *two-spiral-arms* density structure, which may result in a short-term increase in the intensity of the red and blue emission peaks, as observed.

(2) Subsequently, an insight into the "red peak preferential change" may be gained by examining the disparity in the respective densities of the *two-spiral-arms* density structure regions. From the $e = 0$ calculation presented in Panoglou et al. (2016b) figures 4 and 5, the density of the structure on the companion star side is found to exceed that on the opposite side. Thus, if we imagine that the density of the structure on the companion side is higher than that on the opposite side in figure 9, we would expect the red emission peak to be stronger than the blue emission peak ($V/R < 1$), that is, a "red peak preferential change". As illustrated in Figure 5j of Panoglou et al. (2018), the intensity ratio of the Hα emission peaks is $V/R < 1$ for the early phase of the orbital motion (p = 0–0.15) in the edge-on view disk.

The hypothetical *two-spiral-arms* density structure rotating on the Pleione's disk, which is discussed above, also provides insight into the conditions under which a "flat red emission peak," as illustrated in figure 2, may emerge abruptly. This is due to the possibility that during a rotation of the structure, a broad radial velocity contour region exhibiting near-constant density in the outer region of the disk may be temporarily produced. Nevertheless, further investigation is required to provide preliminary evidence for the existence of a *two-spiral-arms* density structure from the observation. For example, during the periastron phenomenon, if variations in the absorption intensities of the metallic shell lines correlate with the "red peak preferential variation" of the Hα line, the density variation in front of the photosphere will be observable, then the reality for the presence of a *two-spiral-arms* density structure can be strengthened. As stated in section 1, the phenomenon of "red peak preferential change" in the Hα line is also synchronous with the variation in the Hβ emission line. However, in this section, the inner region of the disk is not considered, and the region of Hα emission line intensity variation is assumed to be only the outer region of the disk.

5. Summary

This paper presents a detailed analysis of the long-term variation of the Pleione Hα emission line profile over a 14-year period, from 2009 to 2023. The data used in this study were obtained from the BeSS database. The 520 Hα normalised profiles, which were processed in accordance with the methodology outlined in paper I, have been corrected for binary orbital motion. The following three points are discussed.

(1) An examination of the similarity of profile variations after each periastron transit of the companion star, based on the profile variation in figure 2, revealed the following findings: There are similarities in the pattern of variation of the emission line peak region during the 6 years from the maximum of the Be-shell activity to the pre-transition to the Be phase, i.e. for each of the 11 periastron transits of the companion star.

(2) As the Be-shell phase progresses towards the Be phase, the Hα blue emission wing exhibits a strengthening of the wing in comparison to the red emission wing. This trend occurs concurrently with a reduction in the long-term *background* variation V/R ratio of the Hα emission line peak intensity, which is approaching 1 from a maximum value. This suggests the formation of a spiral density wave in the inner region of the disk.

(3) A distinctive profile variation has been documented, wherein the Hα red emission peak is observed to be more pronounced than the blue emission peak ($V/R < 1$) for a brief interval following each transit of the companion periastron. This mechanistic regularity has been consistently recorded over a 10-year period. The mechanism underlying this regularity was discussed in a tentative and qualitative manner, combining various assumptions regarding the position of the companion star periastron on the celestial plane, the disk configuration on the celestial plane, and the appearance of the *two-spiral-arms* density structure on the disk due to the companion star tides. The referenced studies are Hirata (2007) and Panoglou et al. (2016a, b).

Ackowledgment

This work has made use of the BeSS database, operated at LESIA, Observatoire de Meudon, France (http://basebe.obspm.fr). The author wishes to express his hearty thanks to the BeSS database. The author is grateful to the referee for the useful comments, which helped to improve the manuscript. Stimulated by the proof of the existence of the periastron phenomenon by Pollmann and Vollmann (2014), I started to study the data of Pleione in the BeSS database with the help of Drs. R. Hirata (ex-Kyoto University) and S. Honda (University of Hyogo). I learned a great deal from the discussions with both of them at that time. I am deeply grateful to both of them.

References

Cramer, N., Doazan, V., Nicolet, B., de la Fuente, A., & Barylak, M. 1995, A&A, 301,811
Ducati, J. R. 2002, yCat2237
Frémat, Y., Zorec, J., Hubert, A.-M., & Floquet, M. 2005, A&A, 440, 305
Gaia Collaboration (Babusiaux, C., et al.) 2018, A&A, 616, A10
Gontcharov, G. A. 2006, AstL, 32, 759
Hirata, R. 1995, PASJ, 47, 195
Hirata, R. 2007, in ASP Conf. Ser., 361, Active OB-Stars: Laboratories for Stellare and Circumstellar Physics, ed. S. Steflet et al., (San Francisco: ASP), 267
Hirata, R., & Kogure, T. 1978, PASJ, 30, 601
Hummel. W., & Hanuschik, R. W. 1997, A&A, 320, 852
Iliev, L., Kubat, J., Kubatova, B., & Dankova, L. 2023, BlgAJ, 39, 3
Katahira, J. 2023, Stars and Galaxies, 6, 1
Katahira, J., Hirata, R., Ito, M., Katoh, M., Ballereau, D., & Chauville, J. 1996, PASJ, 48, 317
Katahira, J., Maeno, S., Honda, S., & Charbonnel, S. 2020, 第 25 回天体スペクトル研究会集録, 28
Marr, K. C., Jones, C. E., Tycner, C., Carciofi, A. C., & Silva, A. C. Fonseca. 2022, ApJ, 928, 145
Nemravová, J., et al. 2010, A&A, 516, 80
Okazaki, A. T. 1996, PASJ, 48, 305
Okazaki, A. T., Bate, M. R., Ogilvie, G. I., & Pringle, J. E. 2002, MNRAS, 337, 967
Panoglou, D., Carciofi, A. C., Okazaki, A. T., & Rivinius, T. 2016a, in ASP Conf. Ser., 506, Bright Emissaries: Be Stars as Messangers of Star-Disk Physics, ed. T. A. A. Sigut & C. E. Jones, (San Francisco: ASP), 77
Panoglou, D., Carciofi, A. C., Vieira, R. G., Cyr, I. H., Jones, C. E., Okazaki, A. T., & Rivinius, T. 2016b, MNRAS, 461, 2616
Panoglou, D., Faes, D, M., Carciofi, A. C., Okazaki, A. T., Baade, D., Rivinius, T., & Borges Fernandes, M. 2018, MNRAS, 473, 3039
Pearce, J. A., & Hill, G. 1975, PDAO, 14, 319
Poeckert, R., & Marlborough, J. M. 1979, ApJ, 233, 259
Pollmann, E., & Vollmann, W. 2014, BAVSR, 63, 149
Tanaka, K., Sadakane, K., Narusawa, S.-Y, Naito, H., Kambe, E., Katahira, J.-I, & Hirata, R. 2007, PASJ, 59, L35